Contents lists available at ScienceDirect

Chemical Engineering Research and Design

journal homepage: www.elsevier.com/locate/cherd

Improvements of a hollow fiber reverse osmosis desalination model: Analysis of numerical results

*Marian G. Marcovecchio, Nicolás J. Scenna, Pío A. Aguirre**

INGAR Instituto de desarrollo y diseño, Avellaneda 3657, S3002GJC Santa Fe, Argentina

ABSTRACT

In this work, a rigorous model describing the processes taking place in hollow fiber modules for reverse osmosis desalination is analyzed. The Kimura–Sourirajan model is used for describing transport phenomena through the membrane. The concentration polarization phenomenon is mathematically described using the film theory, while the Hagen–Poiseuille and Ergun equations describe the pressure drop in the fiber bore and on the shell side of the fiber bundle, respectively. Improving the previous model, in this work the salt concentration of the permeate accumulated along the fiber is calculated from appropriate mass balances. Hence, the osmotic pressure and the water and salt fluxes through the membrane that depend on this concentration change through the module; and it also influences indirectly the calculation of other process parameters. The solutions of all the differential equations involved in the model are accurately approximated by the finite differences method applied over an appropriate discretization. The value of the output variables changes less than 1% when the finite difference mesh is increased from 6 to 7 grid points in the range of each domain, axial and radial. The flow rates and salt concentrations profiles obtained by the proposed model are analyzed. The influences of the transmembrane and osmotic pressures over the permeate flow rates and salt concentrations are studied. The effect of incorporating the accumulated permeate salinity is showed. It is proved that errors committed by ignoring the permeate accumulated salinity can be significant. Sensitivity analysis for the permeate flow rate and permeate salt concentration is performed by studying the influence of different kind of data: input variables, physical coefficients and design variables.

Keywords: Hollow fiber module; Mathematical modeling; Reverse osmosis

1. Introduction

Reverse osmosis processes have become the separation method most widely used in the production of potable water from brackish and seawater. This process reduces considerably the energy consumption compared to thermal separations. In last years, important research advances have been focused on producing new membranes, improving the flux and rejection processes. Also, efficient energy recovery systems have been developed to reduce the external energy consumption.

The most widely employed membrane configurations for reverse osmosis are hollow fiber, spiral wound, tubular and plate and frame. Hollow fiber modules are currently preferred by many because they have the highest surface area per unit volume and recovery factor.

Important efforts have been focused on modeling the permeation process by resorting to irreversible thermodynamics and transport mechanisms. In particular the reverse osmosis permeation within hollow fiber modules has been studied and mathematically modeled. The Kimura–Sourirajan model (Kimura and Sourirajan, 1967) is widely used to describe the transport phenomena of solute and water through the membrane. This model combines solution-diffusion equations for the transport within the membrane with the film theory for the transport outside the membrane. The model involves two membrane parameters: pure water and salt permeability constants. The principal contribution of this formulation is the modeling of the concentration polarization phenomenon whose influence had been commonly disregarded. Costa and Dickson (1991) developed two models for the design and prediction of the performance of reverse osmosis systems with

* Corresponding author. Tel.: +54 342 4555229; fax: +54 342 4553439.
E-mail address: paguir@santafe-conicet.gov.ar (P.A. Aguirre).
Received 27 April 2009; Received in revised form 9 October 2009; Accepted 10 December 2009
0263-8762/$ – see front matter Published by Elsevier B.V. All rights reserved.
doi:10.1016/j.cherd.2009.12.003

Nomenclature

Subscripts

i	ith grid point along radial direction, variable R
j	jth grid point along axial direction, variable z
ρ^b	brine density, kg/m^3
ρ^p	pure water density, kg/m^3
μ^b	brine viscosity, kg/(m s)
μ^p	permeate stream viscosity, kg/(m s)
$(1/h)$	membrane area per unit volume of fiber bundle, $1/m$
Q^b	brine flow rate inside the shell, m^3/h
Q^{flot}	total feed flow rate, m^3/h
Q^{ptot}	total permeate flow rate, m^3/h
Q^{btot}	total rejected concentrated flow rate, m^3/h
C^{flot}	salt concentration of the total feed stream, ppm
C^{ptot}	salt concentration of the total permeate stream, ppm
C^{btot}	salt concentration of the total rejected stream, ppm
C^b	salt concentration of the bulk flow rate, ppm
C^{pa}	salt concentration of the permeate flow rate accumulated along the fiber, ppm
C^p	salt concentration of the permeate flow rate, ppm
C^m	salt concentration at the membrane wall, ppm
J^w	water flux, kg/m^2 h
J^S	solute flux, kg/m^2 h
ε	void fraction
P^f	feed stream pressure, atm
P^p	pressure in the fiber bore, atm
P^b	pressure on the shell side of the fiber bundle, atm
v^w	velocity of permeation flow, m/h
u^S	superficial velocity in the radial direction of the bulk stream, m/s
A	pure water permeability constant, kg/m^2 s atm
B	solute permeability constant, m/s
D	diffusivity coefficient, m^2/s
d_p	specific surface diameter, m
i	number of ions for ionized solutes
k	mass trasnfer coefficient, m/s
L	length of fiber bundle, m
Ms	solute molecular weight
R	ideal gas constant, N m/(kg mol K)
Re	Reynolds number ($2r_oU_s^S\rho^b/\mu^b$)
Ri	inner radius of the fiber bundle, m
r_i	inner fiber radius, m
Ro	outer radius of the fiber bundle, m
r_o	outer fiber radius, m
Sc	Schmidt number (μ^b/ρ^bD)
Sh	Sherwood number ($2kr_o/D$)
S^M	membrane surface area, m^2
A_m	module membrane area, m^2
T	seawater temperature, K

spiral wound modules: an average and a cell model. Both models employ the Kimura–Sourirajan analysis for spiral wound modules and in both of them the concentration polarization is taken into account.

Another important contribution corresponds to the friction-concentration-polarization model (FCP) (Sekino, 1993). In this work, Sekino incorporates the Kimura–Sourirajan formulation for the transport phenomena of solute and water transport through the membrane. Furthermore, the pressure drop in the fiber bore of a hollow fiber module is taken into account. In a later work, Sekino (1995) compares the FCP model with two until then commonly used models: in one of them the pressure drop in the fiber bore is not taken into account and in the other, the concentration polarization phenomenon is ignored. The FCP model is solved through the finite difference method, discretizing the radial and axial directions. The predictions of the three models are compared against experimental data for different feed concentrations and operating pressures, and the FCP model results the most appropriated one.

Hawlader et al. (1994) investigated the performance of the DuPont B10 hollow fiber permeators. From experimental data the authors studied the product flow rate and concentration as functions of the feed concentration, pressure, temperature and feed flow rate. Later, Malek et al. (1994) introduced a simple model based on a lumped transport parameter approach for modeling the performance of DuPont B10 hollow fiber permeators. The model performs a one-dimensional simplification of the permeator hydrodynamics, considering a linear relationship between the shell side concentration and the membrane surface area.

Starov et al. (1995) presented an analytical model for the hollow fiber membranes. The authors define the fiber performance according to a balance between fiber productivity and fiber selectivity. Three flow configurations modules for reverse osmosis hollow fiber membranes are considered: concurrent, feed outside fibers and feed inside fibers. In a second work Smart et al. (1996), the fiber performance is studied for different fiber geometries and operating parameters.

Al-Bastaki and Abbas (1999) formulated an average and complete model to predict the performance of hollow fiber membranes in reverse osmosis. The model is based on the solution-diffusion model for the mass transport through the membrane and calculates the pressure drop in the fiber bore as well as the pressure drop on the shell side of the fiber bundle. The solution concentration variation on the shell side of the fiber bundle and the concentration polarization are also considered. Later, Al-Bastaki and Abbas (2000) compared theoretical results with experimental data for hollow fiber and spiral wound modules. The effects of ignoring the concentration polarization and the pressure drop are studied. Moreover, a model where the salt and water fluxes are considered as implicit functions of the length and radius module was incorporated and these functions were integrated over the whole module, obtaining better predictions for a set of experimental data.

Marriott and Sørensen (2003a) presented a mathematical model for the separation of a general mixture in a hollow fiber module in parallel flow. Later, Marriott and Sørensen (2003b), extended the model to spiral wound modules and hollow fiber with radial flow. The model incorporates rigorous mass, momentum and energy balances and results are obtained by using the gPROMS simulation software. The model is applied for process simulation and parameter estimation with several cases studies.

Villafafila and Mujtaba (2003) performed several simulations to study the sensitivity of operating and design parameters in a desalination reverse osmosis process using

tubular modules. Then, an optimization was carried out through successive quadratic programming in order to determine the optimal values of operating and design parameters.

Wiley and Fletcher (2003) developed a computational fluid dynamics model of concentration polarization and fluid flow in membrane process. Later, Fletcher and Wiley (2004) extended the model to include a quasi-mechanistic formulation for the membrane transfer process. The model was applied to analyze the effect of buoyancy in salt–water separation in a flat sheet reverse osmosis system.

Chatterjee et al. (2004) extended the friction-concentration-polarization model (Sekino, 1993) for the radial flow in hollow fiber permeators, replacing the solution-diffusion model for the transport phenomenon by the non-linear Spiegler–Kedem model. The principal difference between both models is the incorporation of a third membrane parameter: the reflection coefficient. Numerical solutions were obtained through the finite difference method.

Jamal et al. (2004) proposed a simulation model including material balances in the feed tank, membrane module, product tank and membrane mass transfer models. The proposed model considers spatial dependence of solute feed concentration and shows favorably agreement with actual data.

Paul (2004) proposed a reformulation of the classical solution-diffusion model for reverse osmosis relaxing some assumptions. Potential effects of coupling between solvent and solute transport within the membrane and convective effects are considered.

Avlonitis et al. (2007) used an analytical mathematical model to develop software which predicts the performance of any membrane permeator. The model and software are verified with experimental data from a specific plant and compared with other design softwares.

Recently, Kumano et al. (2008) proposed a hollow Fiber Group Model. The purpose of the new model is to correct an anomaly of the FCP model: the simulated boundary layer thickness results larger than the apparent length of the clearance among hollow fibers. By dividing the mass transfer mechanism that difficulty is overcome. Consequently, the boundary layer thickness on the surface of the fiber group obtained by the application of the Fiber Group Model is smaller than the length of clearance between the fiber groups.

In this work a model for predicting the permeation performance in reverse osmosis seawater desalination with hollow fiber module is presented. The model considers all the most important factors involved in the permeation phenomenon: transport of solute and water through the membrane, concentration polarization, pressure drop in the fiber bore and the pressure drop on the shell side of the fiber bundle, among others.

As other works (Sekino, 1995; Al-Bastaki and Abbas, 2000), the flow velocities and concentrations are considered with radial and axial distribution, as well as the mass transfer coefficient.

Meanwhile the salt concentration of the permeate in each section is obtained from a material balance as usual; in this work the evaluation of the salt concentration of the permeate flow rate accumulated along the fiber is proposed. This concentration is necessary for the direct evaluation of: osmotic pressure and water and salt fluxes through the membrane. Consequently, this concentration affects all the permeation process estimation.

An appropriate finite difference mesh for a hollow fiber module is implemented, dividing the module in its axial and radial directions (Sekino, 1995; Chatterjee et al., 2004). The finite differences method is applied to solve the involved differential equations. The resulting model is completely determined by three operating parameters: flow rate, salt concentration and operating pressure. By fixing these values the model can be solved as a non-linear equations system with unique solution. The number of grid points that keep the approximation error for some variables within an acceptable range is calculated. A thorough analysis of the profiles within the permeator is presented. The effects of incorporating the accumulated permeate salinity are studied by comparing these results with ones achieved when this salinity is ignored. Finally, the influence of the most important parameters on the system performance is discussed through a sensitivity analysis.

The proposed model is used to model the permeation process within a DuPont B10 hollow fiber module. However, it can be applied to other hollow fiber modules, only by setting the appropriate specifications and parameters.

2. Mathematical model

2.1. *Theory equations*

As other works, reverse osmosis membranes arranged as bundles of hollow fibers are here considered (Sekino, 1993; Hawlader et al., 1994; Starov et al., 1995; Al-Bastaki and Abbas, 1999; Chatterjee et al., 2004; Kumano et al., 2008). Dimensions and properties from the DuPont B10 modules are assumed. Fig. 1 shows a module and the internal circulation.

As shown in Fig. 1, the fibers are arranged along the module, in the axial direction. The feed stream enters by a central tube and is distributed through the shell in the radial direction. The fiber bores are sealed at one end and open at the other to allow the permeate to flow out and be collected. The permeate stream flows toward the open end of the fibers, where a porous support and a spacer are located. The concentrated stream is collected by a spacer mesh located outside the fiber bundle.

To formulate the model describing the permeation process with this particular membrane module the following assumptions have been made.

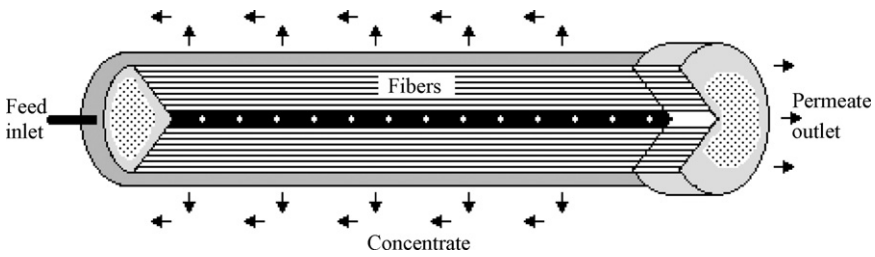

Fig. 1 – Hollow fiber module.

It is assumed that the flow of the bulk stream inside the shell is mainly radial. Thus, null axial velocity is assumed. Indeed, axial permeate flow inside the fibers is assumed. Under these assumptions the partial derivatives in the material balance and the pressure drop equations are replaced by ordinary derivatives.

The pure water and salt permeability are assumed constant parameters within the permeator. Also, it is considered that the permeator has been operating for enough time so stationary state is assumed.

Finally, constant fluid properties as density, viscosity and diffusion coefficient are assumed within the permeator. These assumptions will be relaxed in future works. Particularly, the fluid viscosity dependence on the temperature will be considered.

The basic equations governing the model are established in this section. The model is based on the friction-concentration-polarization (FCP) (Sekino, 1993; Sekino, 1995) that uses the Kimura–Sourirajan model (Kimura and Sourirajan, 1967) for the transport phenomena of solute and water through the membrane. This model has proved to be reliable for predicting the actual module performance at standard conditions and has been widely used (Al-Bastaki and Abbas, 1999, 2000; Kumano et al., 2008).

The brine flow rate inside the shell Q^b can be calculated through the equation of continuity in the bore side, obtained from a material balance for the solution and the solute:

$$\frac{dQ^b}{dr} = -2\pi r L v^w (1/h) \tag{1}$$

The salt concentration of the bulk stream C^b is obtained from a material balance for the salt concentration in the shell side, considering only the convective term:

$$\frac{dQ^b C^b}{dr} = -2\pi r L v^w C^p (1/h) \tag{2}$$

According to the solution-diffusion model (Kimura and Sourirajan, 1967), the water and solute fluxes through the membrane: J^w and J^S, respectively are calculated as

$$J^w = A\,(\Delta P - \Delta\pi) \tag{3}$$

$$J^S = B(C^m - C^p) \tag{4}$$

The osmotic pressure π is calculated with the van't Hoff equation: $\pi = iCRT/Ms$.

The velocity of permeation flow v^w is given by

$$v^w = \frac{(J^w + J^S)}{\rho^p} \tag{5}$$

The salt concentration of the permeate stream C^p in each section is calculated by

$$C^p = \frac{J^S}{v^w \rho^p} \tag{6}$$

An empirical relation involving the Sherwood *Sh*, Reynolds *Re* and Schmidt *Sc* dimensionless numbers is used to calculate the mass transfer coefficient *k* (Al-Bastaki and Abbas, 1999):

$$Sh = 2.725\,(Re)^{1/3}(Sc)^{1/3} \tag{7}$$

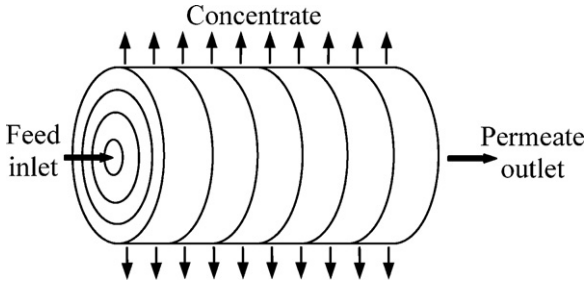

Fig. 2 – Finite difference mesh for a hollow fiber module.

The concentration polarization can be modeled using the solution of the boundary layer equation (Sekino, 1993, 1995; Al-Bastaki and Abbas, 1999, 2000):

$$\frac{C^m - C^p}{C^b - C^p} = \exp\left(\frac{v^w}{k}\right) \tag{8}$$

The Hagen–Poiseuille equation is implemented to calculate the pressure drop in bore side of hollow fiber (Sekino, 1993, 1995; Al-Bastaki and Abbas, 1999, 2000; Chatterjee et al., 2004):

$$\frac{dP^p}{dz} = \frac{8\mu^p Q^p}{\pi r_i^4} \tag{9}$$

The variation in the axial direction of the permeate flow rate Q^p is calculated through the differential equation of continuity in the fiber bore side, as follows:

$$\frac{dQ^p}{dz} = 2\pi r_o v^w \tag{10}$$

By combining the two previous differential equations, the differential equation that calculates the pressure drop in the fiber bore side is obtained:

$$\frac{d^2P^p}{dz^2} = \frac{16\mu^p}{r_i^4} r_o v^w \tag{11}$$

The Ergun equation is used to estimate the pressure drop on the shell side of the fiber bundle (Sekino, 1993, 1995; Al-Bastaki and Abbas, 1999, 2000; Chatterjee et al., 2004):

$$\frac{dP^b}{dr} = \frac{150(1-\varepsilon)^2\mu^b u^S}{\varepsilon^3 d_p^2} + \frac{1.75(1-\varepsilon)\rho^b (u^S)^2}{\varepsilon^3 d_p} \tag{12}$$

The following section describes the finite difference mesh implemented to solve the differential equations using the finite differences method. Then, the equations for the numerical resolution will be detailed.

2.2. *Finite difference mesh for a hollow fiber module*

In this section, the hollow fiber module is discretized adopting the finite difference mesh from Sekino (1995) and Chatterjee et al. (2004) as it is shown in Fig. 2.

According to the hypothesis established in previous section, this mesh is the most appropriated since the process has central symmetry in each module transversal section.

The variable z goes along the permeator: $0 \le z \le L$, meanwhile the variable *R* covers the radial direction: $Ri \le R \le Ro$. The ranges of these two variables are divided in sub-intervals with equal length, although other finite element size distributions perform similarly. The number of intervals used for the partition of z and *R* ranges will be indicated by *m* and *n*, respectively.

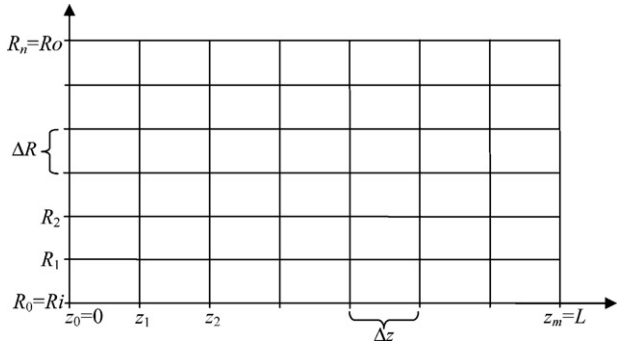

Fig. 3 – Discretization of the axial and radial permeator directions.

Then, if $(n+1)$ points are employed to discretize the R range and $(m+1)$ points to discretize the z range we have:

$$z_0 = 0, \quad z_m = L, \quad z_j = j\Delta z, \quad j = 0, \ldots, m \quad \text{with} \quad \Delta z = \frac{L}{m}$$

and

$$R_0 = Ri, \quad Rn = Ro, \quad R_i = Ri + i\Delta R, \quad i = 0, \ldots, n \quad \text{with}$$
$$\Delta R = \frac{(Ro - Ri)}{n}$$

Fig. 3 shows the discretization mesh in the z–R plane.

Each rectangle in Fig. 3: $[R_i,R_{i+1}] \times [z_j,z_{j+1}]$ represents a ring of the permeator structure: *the permeator fraction comprised between the radius* R_i *and* R_{i+1} *and the lengths* z_j *and* z_{j+1}. In the next section, the equations describing the permeation process taking place in each one of the $n \times m$ rings are established. Each ring of the proposed discretization is represented by the grid point: (z_i,R_j), $j = 1,\ldots,m$; $i = 1,\ldots,n$.

2.3. *Mathematical model: equations for the numerical resolution*

The equations for the numerical resolution of the model described in Section 2.1 are detailed in this section.

In other works, flow velocities and salt concentrations were simplified to only radial variation (Al-Bastaki and Abbas, 1999; Chatterjee et al., 2004). Here, similarly to Sekino (1995) and Al-Bastaki and Abbas (2000), radial and axial dependencies are considered for flow velocities and concentrations as well as for mass transfer coefficient.

The salt concentration of the permeate stream in each section can be obtained from a material balance as usual. However, salt concentration employed for the evaluation of the osmotic pressure and water and salt fluxes corresponds to the permeate flow rate accumulated along the fiber. Consequently, the evaluation of the salt concentration along the fiber is proposed.

Eqs. (13)–(32) describe the process taking place in a reverse osmosis hollow fiber membrane module.

The water flux through the membrane is proportional to the difference between the transmembrane pressure and the osmotic pressure of the feed solution (Kimura and Sourirajan, 1967):

$$J_{i,j}^{w} = 3600\,A\left(P_{i,j}^{b} - P_{i,j}^{p} - \frac{iRT\rho^{b}(C_{i,j}^{m} - C_{i,j}^{pa})}{10^{6}Ms101325}\right)$$
$$i = 1, \ldots, n; \quad j = 1, \ldots, m \qquad (13)$$

where A is the pure water permeability constant, i is the number of ions (for ionized solutes), Ms is the solute molecular weight, R is the ideal gas constant and T is the seawater temperature. P^b and P^p are the pressure on the shell side of the fiber bundle and the pressure in the fiber bore, respectively. C^m is the salt concentration at the membrane wall and C^{pa} is the salt concentration of the permeate accumulated along the fiber. ρ^b is the brine density.

Due to the concentration polarization, the salt concentration at the membrane wall is greater than the brine concentration. The solute flux through the membrane is proportional to the difference between the salt concentration at the membrane wall and the salt concentration of the permeate accumulated along the fiber:

$$J_{i,j}^{S} = \frac{3600B\,(C_{i,j}^{m} - C_{i,j}^{pa})\rho^{b}}{10^{6}} \quad i = 1, \ldots, n; \quad j = 1, \ldots, m \qquad (14)$$

where B is the solute permeability constant.

The velocity of permeation flow is given by equation (15), where ρ^p is the pure water density:

$$v_{i,j}^{w} = \frac{(J_{i,j}^{w} + J_{i,j}^{S})}{\rho^{p}} \quad i = 1, \ldots, n; \quad j = 1, \ldots, m \qquad (15)$$

The salt concentration of the permeate stream in each section is calculated by Eq. (16):

$$C_{i,j}^{p} = \frac{J_{i,j}^{S}10^{6}}{(J_{i,j}^{w} + J_{i,j}^{S})} = \frac{J_{i,j}^{S}10^{6}}{v_{i,j}^{w}\rho^{p}} \quad i = 1, \ldots, n; \quad j = 1, \ldots, m \qquad (16)$$

Eq. (17) represents the discretization of the continuity Eq. (1), using the forward finite differences method. Assuming perfect mixing in each element of the discretization, the finite differences method is the most appropriate to approximate the solutions of the differential equations describing the material balances:

$$Q_{i-1,j}^{b} = Q_{i,j}^{b} + S_{i,j}^{M}v_{i,j}^{w} = Q_{i,j}^{b} + (1/h)\pi(R_i^2 - R_{i-1}^2)\Delta z v_{i,j}^{w}$$
$$i = 1, \ldots, n; \quad j = 1, \ldots, m \qquad (17)$$

L is the length of fiber bundle and $(1/h)$ is the membrane area per unit volume of fiber bundle. $S_{i,j}^{M}$ is the membrane surface area in each module section, thus it is calculated by multiplying the section volume: $\pi(R_i^2 - R_{i-1}^2)\Delta z$ by the membrane surface area per volume unit: $(1/h)$.

It is assumed that the bulk stream inside the shell has positive radial velocity meanwhile the axial velocity is null. Superficial velocity in the radial direction of the bulk stream: u^S is calculated according to Eq. (18):

$$u_{i,j}^{S} = \frac{Q_{i,j}^{b}}{36002\pi R_i \Delta z} \quad i = 0, \ldots, n; \quad j = 1, \ldots, m \qquad (18)$$

Moreover, considering that the brine flow rate in the outer radius of the central tube is the feed: Q^{ftot}, in the inner radius of the fiber bundle this superficial velocity of the bulk stream can also be calculated as

$$u_{0,j}^{S} = \frac{Q^{ftot}}{3600\ 2\pi R_i L} \quad j = 1, \ldots, m \qquad (19)$$

Eqs. (18) and (19) provide the boundary conditions for the continuity Eq. (17).

Eq. (20) is the discretized solution of the convective Eq. (2), using the forward finite differences method, based on the hypothesis of perfect mixing in each element of the discretization:

$$C^{b}_{i-1,j}Q^{b}_{i-1,j} = C^{b}_{i,j}Q^{b}_{i,j} + S^{M}_{i,j}C^{p}_{i,j}v^{w}_{i,j} = C^{b}_{i,j}Q^{b}_{i,j} + (1/h)\pi(R_i^2 - R_{i-1}^2)\Delta z C^{p}_{i,j}v^{w}_{i,j} \quad i = 1,\ldots,n;\ j = 1,\ldots,m \tag{20}$$

In the inner bundle radius, the salt concentration of the bulk stream is the one of the feed stream: C^{ftot}. This is the boundary condition for the convective equation:

$$C^{b}_{0,j} = C^{ftot} \quad j = 1,\ldots,m \tag{21}$$

The permeate flow rate in each section is obtained by multiplying the corresponding membrane area S^M by the velocity v^w. Meanwhile, the salt concentration of the accumulated permeate flow rate is calculated along the fiber. The following equation calculates this salt concentration considering that $S^{M}_{i,j} = (1/h)\pi(R_i^2 - R_{i-1}^2)\Delta z$:

$$C^{pa}_{i,j}\left(\sum_{j=1}^{j}(1/h)\pi\,(R_i^2 - R_{i-1}^2)\Delta z v^{w}_{i,j}\right) = C^{pa}_{i,j-1}\left(\sum_{j=1}^{j-1}(1/h)\pi(R_i^2 - R_{i-1}^2)\Delta z v^{w}_{i,j}\right) + C^{p}_{i,j}(1/h)\pi(R_i^2 - R_{i-1}^2)\Delta z v^{w}_{i,j} \quad i = 1,\ldots,n;\ j = 2,\ldots,m \tag{22}$$

In the first longitudinal sections ($z \in [z_0,z_1]$), there is no accumulation of permeate flow rate. Then, the boundary condition for Eq. (22) is given by

$$C^{pa}_{i,1} = C^{p}_{i,1} \quad i = 1,\ldots,n \tag{23}$$

An important phenomenon to take into account is the concentration polarization. The approach widely used to model the influence of the concentration polarization is the film theory (Kimura and Sourirajan, 1967; Sekino, 1993; Al-Bastaki and Abbas, 1999; Chatterjee et al., 2004). The Sherwood, Reynolds and Schmidt numbers are combined in the empirical relation (7) to calculate the mass transfer coefficient:

$$Sh_{i,j} = \frac{k_{i,j}2r_o}{D} \quad i = 1,\ldots,n;\ j = 1,\ldots,m \tag{24}$$

$$Re_{i,j} = \frac{2r_o\,u^{S}_{i,j}\,\rho^{b}}{\mu^{b}} \quad i = 1,\ldots,n;\ j = 1,\ldots,m \tag{25}$$

$$Sc_{i,j} = \frac{\mu^{b}}{\rho^{b}\,D} \quad i = 1,\ldots,n;\ j = 1,\ldots,m \tag{26}$$

$$Sh_{i,j} = 2.725(Re_{i,j})^{1/3}(Sc_{i,j})^{1/3} \quad i = 1,\ldots,n;\ j = 1,\ldots,m \tag{27}$$

where r_o is the outer fiber radius, D is the diffusivity coefficient and μ^b is the brine viscosity.

Many works performed experimental studies with different membrane modules in order to determine the coefficient and exponent of Reynold's number in Eq. (27). Eq. (27) is taken from Al-Bastaki and Abbas (1999).

Eq. (28) is the discretization of Eq. (8) for modeling the concentration polarization:

$$\frac{C^{m}_{i,j} - C^{p}_{i,j}}{C^{b}_{i,j} - C^{p}_{i,j}} = \exp\left(\frac{v^{w}_{i,j}}{3600\,k_{i,j}}\right) \quad i = 1,\ldots,n;\ j = 1,\ldots,m \tag{28}$$

Eq. (29) is the discretized solution of the differential Eq. (11) obtained through the finite differences method. Since the permeate stream pressure is known at the end of the module, the backward method is applied:

$$P^{p}_{i,j} - P^{p}_{i,j+1} = \frac{16\mu^{p}r_o\Delta z^2}{3600 r_i^4 101325}\sum_{j=1}^{j}v^{w}_{i,j} \quad i = 1,\ldots,n;\ j = 1,\ldots,m-1 \tag{29}$$

μ^p is the permeate stream viscosity and r_i is the inner fiber radius.

The pressure of the permeate stream at the outlet end of the permeator is approximately the atmospheric one. This is the boundary condition for Eq. (29).

$$P^{p}_{i,m} = P_{atm} \quad i = 1,\ldots,n \tag{30}$$

Eq. (31) is the discretization of the Ergun Eq. (12) by the forward finite differences method:

$$P^{b}_{i-1,j} - P^{b}_{i,j} = \left(\frac{150(1-\varepsilon)^2\mu^{b}u^{S}_{i-1,j}}{\varepsilon^3 {d_p}^2 101325} + \frac{1.75(1-\varepsilon)\rho^{b}(u^{S}_{i-1,j})^2}{\varepsilon^3 d_p 101325}\right)\Delta R \quad i = 1,\ldots,n;\ j = 1,\ldots,m \tag{31}$$

ε is the void fraction and d_p is the specific surface diameter.

The pressure value of the bulk stream at the inner radius of fiber bundle is given by the feed stream pressure: P^f. This is the boundary condition for the Ergun Eq. (31):

$$P^{b}_{0,j} = P^{f} \quad j = 1,\ldots,m \tag{32}$$

Eqs. (13)–(32) describe the process taking place at each one of the sections of the membrane module discretization, and the interconnections between them. The objective of this discretized solution is to obtain accurate approximations to the final flow rates, salt concentrations and pressures of the permeate and bulk streams flowing out, for given values of the flow rate, salt concentration and pressure of the stream feed.

From the continuity equation, the flow rate of the permeate stream flowing of the module Q^{ptot} is determined by: $Q^{ptot} = \int_{Ri}^{Ro}\int_0^L v^w dS = \int_{Ri}^{Ro}\int_0^L \frac{1}{h}2\pi R v^w dz dR$ (Al-Bastaki and Abbas, 2000). Thus, the flow rate of the final permeate stream can be estimated by calculating an approximation of the previous integral and using the proposed permeator discretization:

$$Q^{ptot} \cong \sum_{i=1}^{m}\left(\sum_{j=1}^{n}v^{w}_{i,j}S^{M}_{i,j}\right) = \sum_{i=1}^{m}\left(\sum_{j=1}^{n}v^{w}_{i,j}(1/h)(\pi {R_i}^2 - \pi {R_{i-1}}^2)\Delta z\right) \tag{33}$$

The salt concentration of the permeate stream flowing out of the module: C^{ptot} is calculated through a salt material balance: $C^{ptot}Q^{ptot} = \int_{Ri}^{Ro}\int_0^L C^p v^w dS = \int_{Ri}^{Ro}\int_0^L 1/h\,2\pi R C^p v^w dz dR$.

Then, Eq. (34) estimates the salt concentration of the permeate stream by calculating an approximation of the previous integral over the proposed module discretization:

$$C^{ptot} \cong \left(\sum_{i=1}^{m} \left(\sum_{j=1}^{n} C^{p}_{i,j} v^{w}_{i,j} S^{M}_{i,j} \right) \right) / Q^{ptot}$$
$$= \left(\sum_{i=1}^{m} \left(\sum_{j=1}^{n} C^{p}_{i,j} v^{w}_{i,j} (1/h)(\pi {R_i}^2 - \pi {R_{i-1}}^2) \Delta z \right) \right) / Q^{ptot} \quad (34)$$

Eq. (35) is the total material balance for the permeator, where Q^{ftot} and Q^{btot} are the flow rates of the feed and rejected concentrated streams, respectively:

$$Q^{ftot} = Q^{btot} + Q^{ptot} \quad (35)$$

Finally, Eq. (36) is the total mass balance for the salt, where C^{btot} is the salt concentration of the total rejected stream:

$$C^{ftot} Q^{ftot} = C^{ptot} Q^{ptot} + C^{btot} Q^{btot} \quad (36)$$

The finite differences method over an appropriated mesh has been applied to solve the differential equations involved in the reverse osmosis permeation process. The accumulated permeate salinity has been calculated and incorporated in the equations modeling the process. The resulting model is a nonlinear equations system that can be solved provided that the three parameters: flow rate, salt concentration and operating pressure are fixed. In the following section the optimal number of grid points in the discretization is determined, in order to reduce the approximation error to acceptable values. Subsequently, salt concentrations and flow rates inside the module are analyzed.

3. Determination of the number of discretization grid points

Eqs. (13)–(32) describe the phenomena taking place in one membrane module, as a function of the flow rate, salt concentration and pressure of the feed stream. In this section, the number of necessary grid points for the hollow fiber module discretization described in Section 2.3 will be determined, in order to achieve errors in the final values of flow rates, salt concentrations and pressures minor or equal that 1% when the number of grid points is increased in one for each domain. In turn, the number of grid points will determine the amount of variables and equations in the model. Consequently, a very refined mesh will considerably increase the problem size. Then, it is important to find the minimal quantity of grid points that satisfy the imposed error requirement.

With this objective, the problem describing the process in one membrane module was solved for different operating conditions and feed seawater characteristics. That is, the problem defined by Eqs. (13)–(32) was solved fixing the pressure, salt concentration and flow rate of the feed stream at several representative values. These three parameters determine the process, then the complete phenomenon occurring in the permeator is established, and the outlet stream characteristics can be satisfactorily determined.

Therefore, the solutions for the system described by Eqs. (13)–(32) are analyzed for different values of the variables: Q^{ftot}, P^{f} and C^{ftot}, and for increasing numbers of grid points in the process discretization. The characteristics of the outlet streams are compared, in order to achieve the desirable precision. The chosen amount of grid points will be the one showing that the trend of the outlet stream characteristics are practically stabilized, with respect to the solutions obtained through increasing refinements. That means, it is required that the difference between the solutions produced by the chosen discretization and the ones produced by a greater refinement be less than 1% for the values describing the outlet streams.

Table 1 – Parameters for the reverse osmosis desalination model.

Parameters for the reverse osmosis desalination model	
i, number of ions for ionized solutes	2
R, ideal gas constant, N m/kg mol K	8315
Ms, molecular weight of solute	58.8
T, seawater temperature, °C	25
ρ^{b}, average brine density, kg/m^3	1060
ρ^{p}, average pure water density, kg/m^3	1000
μ^{p}, permeate viscosity, kg/m s	0.9×10^{-3}
μ^{b}, brine viscosity, kg/m s	1.09×10^{-3}
D, diffusion coefficient, m^2/s	1×10^{-9}

Table 1 contains the constants and parameters employed in the model resolution.

Table 2 details the specifications of the DuPont B10 hollow fiber module taken from Al-Bastaki and Abbas (1999). These values constitute constants and bounds for some variables of the problem to be solved.

It is acceptable to assume that when the hollow fiber module operates at optimal conditions its feed flow rate is about the maximum allowed value. Then, Q^{ftot} (feed flow rate) was fixed at its maximum allowed value: 0.917 m^3/h for all the solved cases.

The allowed pressure range for the permeator operation is [54.48 atm, 67.90 atm]. Therefore, the three representative values of the operating pressure: P^{f} = 55, 60, 65 atm were considered for the comparative analysis.

The third variable to be fixed is the salt concentration of the feed stream: C^{ftot}. Even though seawater salinity can take values around 35,000–45,000 ppm approximately, higher values for C^{ftot} must be also considered. In fact, a typical reverse osmosis desalination network will be composed of two or more reverse osmosis stages operating in series. Then, seawater salinity will correspond to the feed of the first reverse osmosis stage. But the salinity of the stream entering to other reverse osmosis stage will be the salt concentration of the previous stage rejected stream. It is expected that these

Table 2 – DuPont B10 hollow fiber parameters.

DuPont B10 hollow fiber parameters	
A, pure water permeability constant, kg/m^2 s atm	4.3508955×10^{-5}
B, salt permeability constant, m/s	4.0×10^{-9}
Ri, inner radius of the fiber bundle, m	1.27×10^{-2}
Ro, outer radius of the fiber bundle, m	5.334×10^{-2}
L, length of fiber bundle, m	0.75
A_m, membrane area, m^2	152
r_i, inner fiber radius, m	2.1×10^{-5}
r_o, outer fiber radius, m	5.0×10^{-5}
ε, void fraction	0.4
d_p, specific surface diameter, m	1.2×10^{-4}
Operating pressure range, bar	55.2–68.8
Maximum brine flow rate, m^3/h	0.917

Table 3 – Solutions for different refinements of the membrane module discretization.

Outlet variables per module for different mesh sizes

Inlet stream characteristics									
C^{ftot} (ppm)	35,000	35,000	35,000	45,000	45,000	45,000	55,000	55,000	55,000
P^{f} (atm)	55	60	65	55	60	65	55	60	65
Q^{ftot} (m^3/h)	0.917	0.917	0.917	0.917	0.917	0.917	0.917	0.917	0.917
Q^{ptot} (m^3/h)									
$n=m=1$	0.263	0.307	0.347	0.159	0.203	0.245	0.072	0.113	0.155
$n=m=2$	0.277	0.324	0.367	0.168	0.216	0.261	0.077	0.121	0.166
$n=m=3$	0.282	0.331	0.375	0.172	0.221	0.267	0.079	0.124	0.170
$n=m=4$	0.285	0.334	0.380	0.173	0.223	0.270	0.079	0.125	0.172
$n=m=5$	0.286	0.336	0.383	0.174	0.225	0.272	0.080	0.126	0.173
$n=m=6$	0.288	0.338	0.385	0.175	0.226	0.274	0.080	0.127	0.174
$n=m=7$	0.288	0.339	0.386	0.176	0.226	0.275	0.080	0.127	0.175
C^{ptot} (ppm)									
$n=m=1$	429.7	395.4	374.8	783.3	652.4	576.5	1858.2	1256.3	976.8
$n=m=2$	390.7	356.6	335.9	721.6	596.2	523.3	1724.1	1157.2	894.4
$n=m=3$	375.5	341.2	320.1	699.3	575.2	502.8	1680.8	1122.9	864.5
$n=m=4$	367.5	332.9	311.6	687.8	564.1	491.9	1659.3	1105.3	848.9
$n=m=5$	362.5	327.7	306.3	680.7	557.2	485.1	1646.4	1094.6	839.3
$n=m=6$	359.1	324.2	302.6	676.0	552.6	480.5	1637.9	1087.5	832.8
$n=m=7$	356.7	321.6	300.0	672.6	549.2	477.2	1631.8	1082.3	828.1
$P^{b}_{n,1}$(atm)									
$n=m=1$	54.93	59.93	64.93	54.93	59.93	64.93	54.93	59.93	64.93
$n=m=2$	54.95	59.95	64.95	54.95	59.95	64.95	54.95	59.95	64.95
$n=m=3$	54.96	59.96	64.96	54.96	59.96	64.96	54.96	59.96	64.96
$n=m=4$	54.96	59.96	64.96	54.96	59.96	64.96	54.96	59.96	64.96
$n=m=5$	54.97	59.97	64.97	54.96	59.97	64.97	54.96	59.96	64.96
$n=m=6$	54.97	59.97	64.97	54.97	59.97	64.97	54.96	59.97	64.96
$n=m=7$	54.97	59.97	64.97	54.97	59.97	64.97	54.97	59.97	64.97

salinities reach high values around 50,000 and 60,000 ppm, approximately. Thus, the variable C^{ftot} was fixed at three representative values: 35,000, 45,000 and 55,000 ppm for the comparative analysis.

The study cases resulting from the different values assigned to the three determinant variables are nine. The variables compared for the different mesh refinements are: the permeate flow rate Q^{ptot}, the salt concentration of the permeate stream C^{ptot} and the pressure of the rejected brine stream P^{b}. The flow rate and salt concentration of the rejected stream are not analyzed since these values are complementary to the permeate stream ones. On the other hand, the rejected stream pressure is considered because it could be the operating pressure of subsequent permeators stage.

The range for the radial variable R is $[Ri,Ro] = [1.27 \times 10^{-2}\ m, 5.334 \times 10^{-2}\ m]$, and the range for the axial variable z is $[0,L] = [0\ m, 0.75\ m]$. Even though the axial range is longer than the radial one, the phenomenon in the radial direction is more significant. Here, a mesh with equal number of grid points in each direction was adopted. Thus, the step in z: Δz will be larger than the step in R: ΔR.

Different cases for increasing grid points were solved in turn, until the convergence for the analyzed variables was reached with errors lower than 1%.

Table 3 shows the values of the analyzed variables for all the solved study cases. As it is showed in Table 3, the solutions converge when the mesh is refined. Specifically, considering the solutions obtained for $n=m=7$, the approximation improvement is lower than 0.9% when they are compared to the solutions obtained for $n=m=6$. Such refinement is not necessary to reach the required precision for the pressure of the rejected brine stream, but fewer grid points are not enough to calculate accurately the other considered variables.

The non-linear equations systems were solved with the software GAMS (Brooke et al., 1997), by using the local solver GAMS/CONOPT.

Therefore, 7 points in the discretization of each range, that is $n=m=6$, are enough to fit the required precision. The discretization consists on the partition of each range into 6 sub-intervals of equal length: $\Delta z = 0.125$ m and $\Delta R = 0.6773 \times 10^{-2}$ m. In consequence, the whole module is divided in 36 sections, and all the variables describing the process are approximated in each section.

Models previously proposed like Al-Bastaki and Abbas (1999) and Marcovecchio et al. (2005) are based in the same theoretic equations, but no discretization is employed to solve the involved differential equations. These models correspond to the case $n=m=1$ in the model proposed here. That means: the permeator is considered as a single element and average pressure drops and velocities are estimated. The error in that simplified resolutions can be calculated by comparing the values showed at Table 3 for $n=m=1$ and $n=m=7$ (the best estimation available). For the pressure of the rejected brine stream P^{b} with $n=m=1$ the values estimated are very precise; the relative error goes from 0.06 to 0.07%. However, the relative errors committed with $n=m=1$ for the permeate flow rate Q^{ptot} are significant; in this case they go from 8.7 to 11.4%. Even worse is the approximation for the salt concentration of the permeate stream C^{ptot}: the relative errors are between 13.8 and 24.9%. It is important to note that the estimation provided by considering the whole module as a single element underestimate the permeator permeation performance, since it predicts lower rejected brine stream pressure and permeate flow rate and higher permeate stream salinity.

In order to show the feasibility of the proposed model, it was applied to estimate the performance of a B10 (6440-

Table 4 – Comparing model results with experimental data.

Comparing model results with experimental data (Hawlader et al., 1994)
Inlet stream characteristics
$Q^{ftot} = 1.134\ m^3/h$

C^{ftot} (ppm)	P^f (bar)	Product recovery	
		Experimental	Model results
0	35.5	27%	29%
0	49.5	38%	41%
0	63.1	51%	53%
0	69.9	60%	59%
		Salt rejection	
		Experimental	Model results
25,000	56.16	98.8%	98.2%
25,000	63.05	98.9%	98.4%
25,000	69.95	99.0%	98.5%
25,000	76.84	99.1%	98.6%
30,000	56.16	98.4%	98.0%
30,000	63.05	98.7%	98.3%
30,000	69.95	98.8%	98.4%
35,000	76.84	98.8%	98.4%
40,000	56.16	97.5%	97.3%
40,000	63.05	98.1%	97.8%
40,000	69.95	98.4%	98.1%
45,000	56.16	97.1%	96.7%
45,000	76.84	98.5%	98.1%
50,000	63.05	97.2%	96.9%
50,000	69.95	97.9%	97.6%

T) hollow fiber module. Experimental data for this module for different operating conditions are detailed in Hawlader et al. (1994) and Marriott and Sørensen (2003b). The analysis to determinate the number of discretization grid points was carried out as before, giving $n = m = 8$ to fit the required precision. Table 4 compares the results obtained by applying the model proposed here with experimental data. The model shows satisfactory agreement with the real data, specifically, the error average is 4% for the product recovery calculation, and 0.5% for the salt rejection calculation.

In the following section some salt concentrations and flow rates inside the module obtained for different refinements are analyzed.

4. Results and discussion

4.1. *Profiles inside the membrane module*

From the solutions of the discretized model for different operating conditions and seawater characteristics, the flow rate and salt concentration profiles inside the permeator can be drawn.

As an example, the profiles obtained for the membrane module operating under the following conditions will be shown: feed flow rate at the maximum allowed value: $Q^{ftot} = 0.917\ m^3/h$, feed stream salt concentration at an intermediate value: $C^{ftot} = 45{,}000$ ppm and three representative values for the operating pressure: $P^f = 55$, 60, 65 atm.

Firstly, the curves drawn are the profiles given by the permeate flow at each point along the module for the radius: inner *Ri*, medium (*Ri* + *Ro*)/2 and outer *Ro*. Figs. 4–6 show the

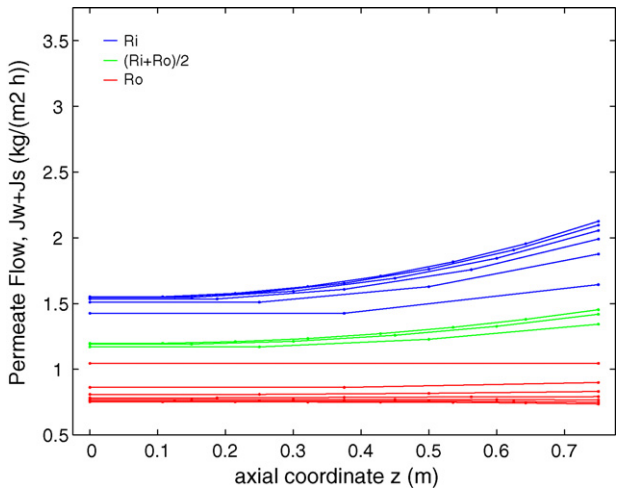

Fig. 4 – Flow profiles along the membrane module for increasing mesh refinements, $P^f = 55$ atm.

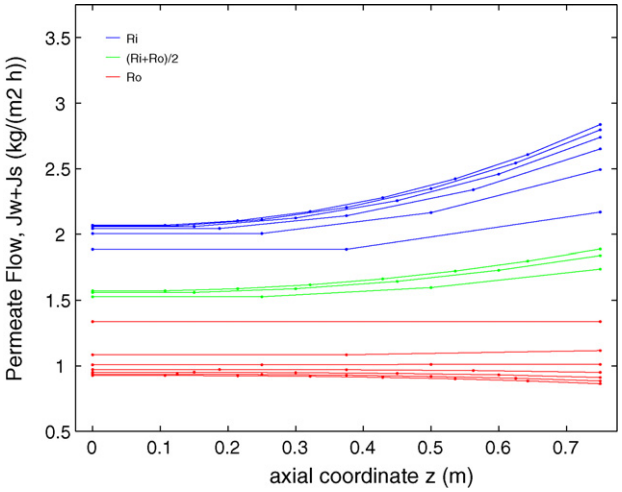

Fig. 5 – Flow profiles along the membrane module for increasing mesh refinements, $P^f = 60$ atm.

curves obtained for 55, 60 and 65 atm of operating pressure, respectively.

The curves correspond to the different mesh refinements, from $n = m = 1$ to $n = m = 7$. For the medium radius, only the profiles obtained with $n = m = 3$, $n = m = 5$ and $n = m = 7$ were drawn,

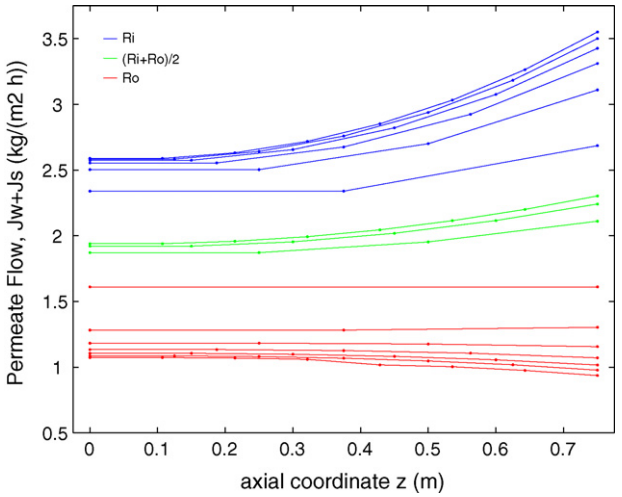

Fig. 6 – Flow profiles along the membrane module for increasing mesh refinements, $P^f = 65$ atm.

since they are the unique containing this radius as a grid point. Similarly to Table 3, the convergence of the solutions when the mesh is refined can also be appreciated in Figs. 4–6.

As can be expected, higher operating pressure, increase permeate flows in all the points. Figs. 4–6 show the relative increments. Moreover, considering a transversal section, that is: for a fixed value of the axial variable z, the permeate flow decreases from a high value in the inner radius toward a lower value in the outer radius. This is mainly due to the values reached by the osmotic pressure and the pressure on the shell side of the fiber bundle, since the permeate flow is proportional to the difference between these two pressures. The pressure on the shell side of the fiber bundle is higher in the inner radius and decreases along the radial direction. The bulk flow gains salinity through in the radial direction; it goes from the feed salt concentration in the inner radius, until a high value in the external radius, as a consequence of the permeate flow rate. Even though the salinity at the membrane surface is always higher than the salt concentration of the bulk, the behavior is similar. Therefore, the osmotic pressure is lower in the inner radius and it increases toward the external radius.

At the inner radius, the permeate flow takes its lowest value at $z=0$ and the highest one at $z=L$, due to the transmembrane pressure difference. In fact, the pressure in the fiber bore takes the value of 1 atm at the open end: $z=L$ and reaches its maximum value at the closed end of the fiber: $z=0$. Thus, the transmembrane pressure difference is greater at $z=L$, producing the highest permeate flow at this point.

From the figures, it can also be appreciated that the curve behaviors from $z=0$ to $z=L$ change from an increasing functionality at the inner radius to a decreasing shape at the outer radius; because near the extreme $z=L$, the influence of the osmotic pressure is more important at the outer radius, where the salt concentration at the membrane surface is high. In fact, toward the outer radius, the transmembrane pressure ($P^b - P^p$) falls because the pressure on the shell side of the fiber bundle is falling, and the salt concentrations difference: ($C^m - C^{pa}$) rises, as a consequence of the considerable rise of the salt concentration at the membrane surface. This causes that the effect of the osmotic pressure variation be more significant at the outer radius, and thus the permeate flow decays, since it is proportional to the difference between the transmembrane and osmotic pressures.

Note that the estimation obtained with $n=m=1$ produces a value for the permeate flow which is intermediate between the maximum and minimum values reached at the inner and outer radius, respectively.

In second place, the drawn curves are the salt concentrations of the permeate accumulated along the module for the radius: inner *Ri*, medium $(Ri+Ro)/2$ and outer *Ro*. Figs. 7–9 show the profiles for 55, 60 and 65 atm of operating pressure, respectively.

Again, the drawn profiles are the ones obtained through increasing refinements from $n=m=1$ to $n=m=7$, and only the curves for meshes containing the medium radius as grid point were drawn in this case.

The curves show similar global behavior for the three values of the operating pressure. It can be appreciated that the salt concentration of the permeate is higher when the module operates at low pressure; and as the operating pressure increases a permeate stream with lower salt concentration is obtained.

The permeate salt concentration is lower in the inner radius, and it rises toward the outer radius. That is a straight consequence of the permeation process. In fact, the brine flows mainly in the radial direction, entering with the salt concentration of the feed stream at the inner radius. If a radius greater than the inner one is considered, the salt concentration of the bulk will be higher, as a consequence of the amount

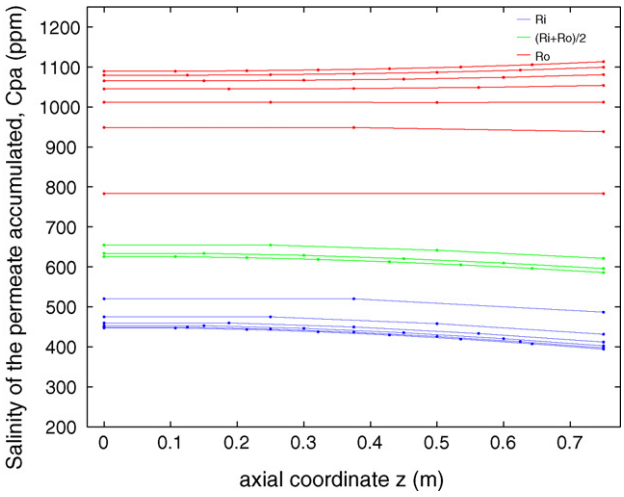

Fig. 7 – Profiles of the permeate salinity along the module for increasing mesh refinements, $P^f = 55$ atm.

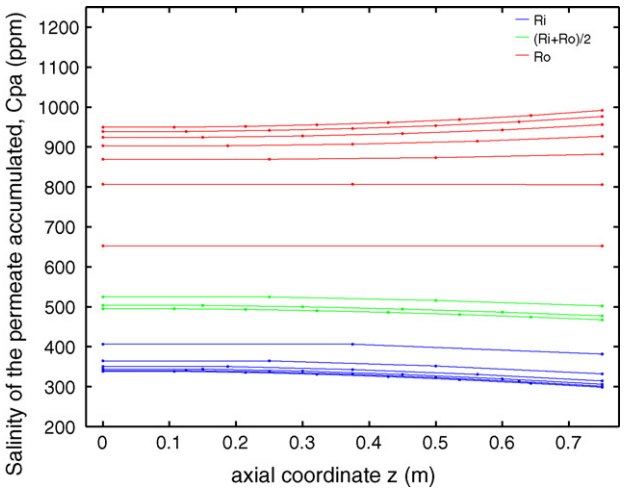

Fig. 8 – Profiles of the permeate salinity along the module for increasing mesh refinements, $P^f = 60$ atm.

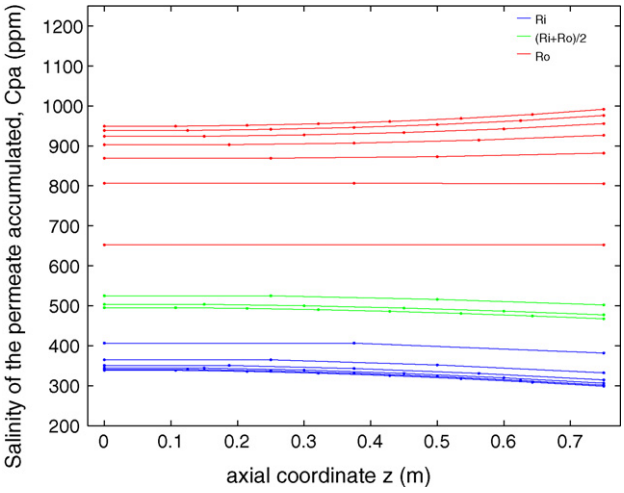

Fig. 9 – Profiles of the permeate salinity along the module for increasing mesh refinements, $P^f = 65$ atm.

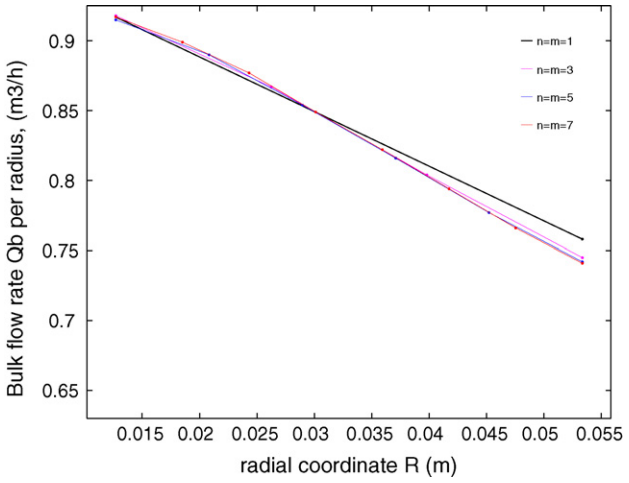

Fig. 10 – Bulk flow rate sum per radius for increasing mesh refinements, $P^f = 55$ atm.

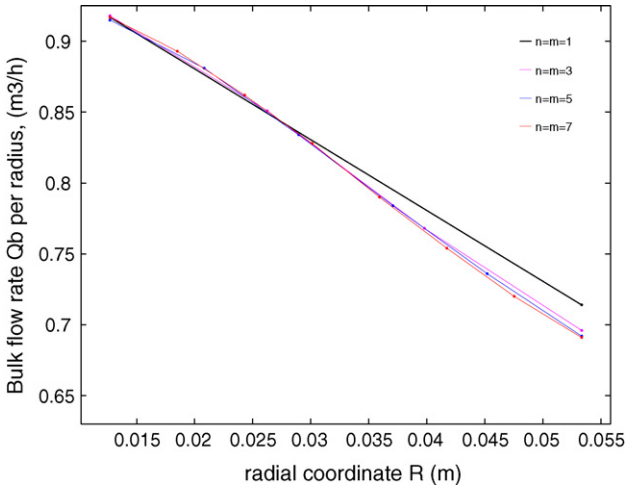

Fig. 11 – Bulk flow rate sum per radius for increasing mesh refinements, $P^f = 60$ atm.

that has been permeated in the section going from the inner radius until the radius in consideration. Then, the flow permeated at that radius will have salt concentration higher than the one permeated at the inner radius, since the bulk is more concentrated.

Furthermore, the figures show that curve shapes from $z = 0$ to $z = L$ change from a slightly decreasing functionality at the inner radius to a slightly increasing shape at the outer radius. As it were explained previously, at the radius Ri the permeate rises toward $z = L$ mainly influenced by the transmembrane pressure drop, since at $R = Ri$ and $z = L$ the difference $(P^b – P^p)$ reaches its maximum value; and in second place, by the osmotic pressure drop which is measured by the difference $(C^m - C^{pa})$. Therefore, the permeate flow at the inner radius and near the extreme $z = L$ consists principally of fresh water. Then, the salt concentration of the accumulated permeate falls along the inner radius from $z = 0$ to $z = L$. Moreover, as it was mentioned, toward the outer radius and the extreme $z = L$, the influence of the osmotic pressure is more important, since the salt concentration of the membrane surface rises considerably. Then, the permeate salt flow, which is proportional to the difference $(C^m - C^{pa})$, increases. However, as Figs. 4–6 show, the total permeate flow diminishes. This explains the slight increase of the salt concentration of the accumulated permeated near the radius Ro and toward the extreme $z = L$.

Note that the discretization using $n = m = 1$ estimates the salt concentration of the permeate as an intermediate value between the maximum and minimum concentrations reached at the outer and inner radius, respectively.

Finally, the profiles given by the rejected stream: Q^b are presented. That is, the curves show the summation performed from $z = 0$ to $z = L$ of the bulk flow rate at each radius, for increasing discretization refinements. Figs. 10–12 show curves for 55, 60 and 65 atm of operating pressure, respectively. In this case, for more clarity, only the curves obtained for n and m having odd values are presented.

At the inner radius, the bulk stream consists of the feed stream to the permeator. From $R = Ri$ to $R = Ro$, the bulk stream flow rate diminishes because of the stream partially permeated. Considering Figs. 10–12, it can be concluded that the permeation process is more efficient at high operating pressure. That is, the permeate flow rate will be higher at low salt concentration and consequently, the bulk flow rate will be lower.

For the three values of the operating pressure, the curve of the bulk stream flow rate changes its concavity at a value close to the medium radius: $(Ri + Ro)/2$. This behavior agrees with the analysis for the flow rate and salt concentration of the permeate. The inflexion point marks the radius for which the profiles of the permeate change from increasing to decreasing functionality, when the radius goes from Ri to Ro (Figs. 4–6). As it was explained, the influence of the transmembrane pressure drop is major at the radius Ri, meanwhile at the radius Ro the permeation process is dominated by the osmotic pressure. The inflexion point is the radius where the process passes from obeying mainly to the transmembrane pressure drop to be influenced principally by the osmotic pressure drop.

4.2. *Effects of incorporating the accumulated permeate salinity*

In the present section, the salinity of the permeate stream is compared to the salinity of the accumulated permeate stream along the fiber. A representative case is analyzed. Fig. 13 shows both: the permeate and accumulated permeate salinities for 45,000 ppm of feed salt concentration, when the module is operated at maximum pressure: 67.9 atm and feed brine flow rate: 0.917 m^3/h. The mesh refinement employed is $n = m = 7$.

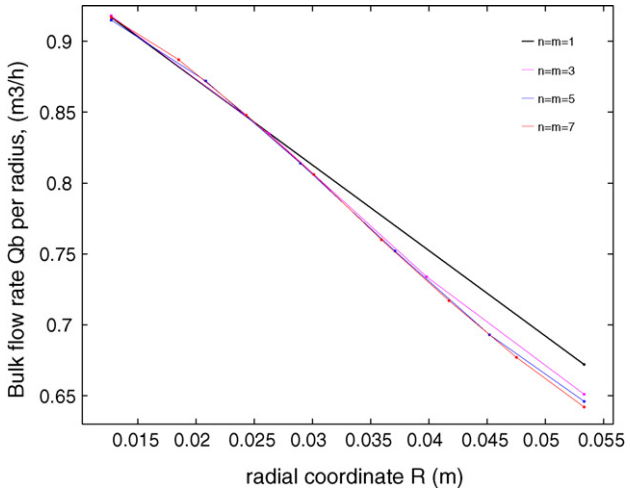

Fig. 12 – Bulk flow rate sum per radius for increasing mesh refinements, $P^f = 65$ atm.

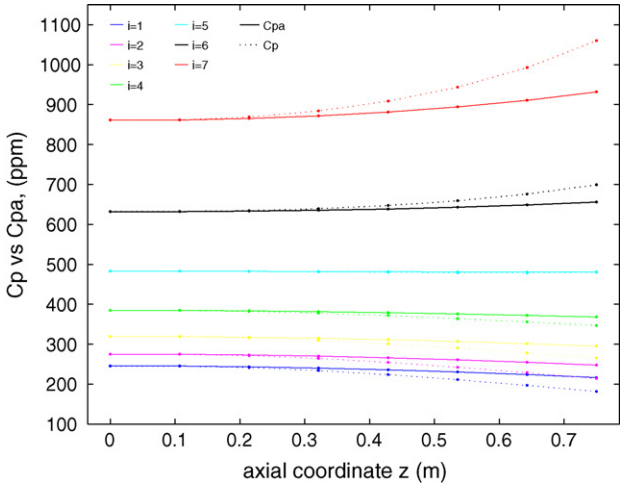

Fig. 13 – Permeate vs. accumulated permeated salinities.

As can be expected, both salinities are almost coincident at the initial extreme of the fiber, approximately for $z \in [0\,m, 0.2\,m]$. The general behavior of both concentrations is similar: The permeate salt concentration is lower in the inner radius, and it rises toward the outer radius; and the curve shapes from $z = 0$ to $z = L$ change from a slightly decreasing functionality at the inner radius to a slightly increasing shape at the outer radius.

However, from Fig. 13 is evident the discrepancy between both salinities. The difference between C^p and C^{pa} increases when z goes from 0.2 m to the final extreme: 0.75 m. That difference reaches up to 16% of the C^{pa} value. Moreover, the increasing/decreasing functionalities are more pronounced for the salinity of the permeate at each section. Then, the calculation of the salt concentration of the permeate accumulated along the fiber is imperative if a precise model for the permeation process is desired.

Nevertheless, if the final characteristics of the product are considered, the effect of incorporating the permeated accumulated salinity is not significant. In fact, for several solved cases the maximum errors committed by ignoring that salinities is 0.4% for the salt concentration of the total permeate stream and 0.5% for the total permeate flow rate.

The proposed model has been applied to estimate the permeation process through reverse osmosis with the DuPont B10 hollow fiber permeator. But the model can be also applied to estimate the permeation for other hollow fiber modules, assuming that the specifications and parameters characterizing the permeator are available. In that case, the errors committed by ignoring the permeate accumulated salinity can be significant, especially if the fiber bundle is longer. From Fig. 13 it can be predicted that the difference between the permeate and accumulated permeate salinities will increase for longer fiber, and as a consequence higher error for the final product characteristics can be obtained.

4.3. *Sensitivity analysis*

In this section, the effect of increasing or decreasing some model parameters is studied. Despite the fact that the problem to be solved is a non-linear equations system, the software for mathematical programming and optimization: GAMS (Brooke et al., 1997) was implemented for the resolution, by using the local solver GAMS/CONOPT. After the resolution, one of the solver output is the marginal values for each variable and equation. That is one of the advantages of implementing that optimization software and it will be explored here.

Table 5 – Relative marginal values for the flow rate and salinity of the total permeate stream.

Sensitivity analysis

Inlet stream characteristics

C^{ftot} (ppm)	45,000
P^f (atm)	67.9
Q^{ftot} (m^3/h)	0.917

Relative marginal values

$(\partial Q^{ptot}/\partial p)(p/Q^{ptot})$		$(\partial C^{ptot}/\partial p)(p/C^{ptot})$	
P^f	2.0151	C^{ftot}	2.0451
T	−1.5690	Ro	−1.5429
C^{ftot}	−1.5688	P^f	−1.3051
L	−1.0011	T	1.0452
Ro	−0.9336	B	0.9753
Q^{ftot}	0.5607	Ri	0.8171
Ri	−0.5078	Q^{ftot}	−0.7296
A_m	0.4403	A_m	0.7277
A	0.3365	A	−0.1924
r_i	0.3164	r_i	−0.1907
r_o	−0.0829	r_o	0.0526
B	0.0191	L	0.0019

When an optimization problem is solved, a variable: the objective function is minimized or maximized. Let y be the objective function. The marginal value of a variable x, also kwon as dual variable or Lagrangian multiplier, is defined as: $\partial y/\partial x$ evaluated at the optimal value. This partial derivative considers all the explicit and implicit influence of the variable x over the variable y, given by the proper objective function definition as well as the model equations.

The marginal values for a representative example are presented. The solved case corresponds to 45,000 ppm of feed salt concentration, 67.9 atm of operating pressure and 0.917 m^3/h of feed flow rate. The mesh refinement employed is $n = m = 7$. Table 5 shows the relative marginal values for the flow rate and salt concentration of the total permeate stream, that is: $(\partial Q^{ptot}/\partial p)(p/Q^{ptot})$ and $(\partial C^{ptot}/\partial p)(p/C^{ptot})$ for the main model parameters. The relative marginal values are more appropriated to evaluate the influence of the change at each variable over the whole process. Note that operating conditions (P, T, C, Q) physical parameters (A, B, A_m) and design parameters (L, r_o, r_i, Ro, Ri) are investigated. All of these parameters are defined as "variables" in the GAMS models, and their values are fixed before solving the models. In this way, the solver computes the numerical derivative for the objective function and constraint with respect to these fixed variables and reports their values at optimality.

The relative marginal values are arranged according their absolute values. The positive sign of a relative marginal indicates that the objective function increases its value when the corresponding parameters are increased. On the contrary, a negative relative marginal indicates that increasing the parameter decreases the objective value. The marginal value tell as by at most how much we can benefice modifying a particular parameter. Then, if a parameter p is increased from its current value p^* by a small amount: Δp, the net change for the objective function y will be: $(\Delta p \partial y/\partial p)$ approximately.

As Table 5 shows, the operating pressure is the parameter more influential over the permeate flow rate. It would be profitable to increase the operating pressure, in case it is possible, in order to obtain higher permeate flow rate. At the same

time, increasing this parameter would diminish the salt concentration of permeate stream. Contrarily, and even though the feed salinity is not always a parameter feasible to manipulate, its rise would produce lower permeate flow rate with higher salinity.

The effect of a rise in the feed temperature is negative to decrease the salintity of the permeate stream as well as to increase its flow rate. Note that for the porposed model, the feed temperature is affecting only the osmotic pressure. Extending the fiber bundle is detrimental for the permeate flow rate, but it would not affect the permeate salinity.

In that way, the effect of increasing or decreasing each parameter can be evaluated and considered, according the persued objective. Also, information about wich parameters do not incluence the objective can be obtained. In that way, the implementation of sensitivity analysis as a powerfull tool to evaluate changes in the design and operating conditions of a particular permeator has been described and exemplified.

5. Conclusions

This work presents a rigorous model for the permeation process taking place in a hollow fiber membrane module for reverse osmosis desalination.

With this aim, an appropriated discretization of the permeator has been implemented. By using the discretization, the solutions of the involved differential equations have been approximated through the finite differences method. The number of grid points was proposed in order to guarantee incremental errors lower than 1% for each final variable. That led to a finite difference mesh with 7 grid points in the range of each discretized variable. Then the module was divided into 36 sections, and the permeation process was approximated in each one of these sections. It was showed that the relative errors committed when no discretization is implemented are significant. Without discretization, the relative errors reach up to 11.4% for the permeate flow rate and 24.9% for the salt concentration of the permeate stream. Then, accurate calculations are necessaries in order to estimate appropriately the permeation module performance.

The profiles for the flow rates and salt concentrations inside the module have been studied with the proposed model. An analysis of the influence of the transmembrane and osmotic pressures over the permeate flow rates and salt concentrations was carried out. The accumulated permeate salt concentration falls along the inner radius from $z = 0$ to $z = L$ whereas the accumulated permeate salt concentration slight increases near the extern radius Ro from $z = 0$ toward the extreme $z = L$. This behavior is caused by the salt fluxes that depend on the values of the transmembrane pressure difference and the osmotic pressure difference. Analogue behavior is obtained for the permeate flow rate.

In the present work the evaluation of the salt concentration of the permeate flow rate accumulated along the fiber is proposed. This concentration affects the calculation of the osmotic pressure and the water and salt fluxes through the membrane and its influence has been studied. If the final exit characteristics are considered, the effect of incorporating the salinity of the permeate accumulated is not significant for the particular adopted permeator. However, it has been showed that the difference between the salinities of the permeate stream and the accumulated permeate stream along the fiber is considerable: it reaches up to 16% in some partes of the device (see Fig. 13). Moreover, it can be predicted that the errors commited by ignoring the salinity of the permeate accumulated can be considerable if longer permeator are studied. Then, higher error for the final product characteristics can be introduced when the length and the diameter of the permeator are varied. Therefore, the calculation of the salt concentration of the permeate accumulated along the fiber should not be disregarded in order to model the permeation process accurately.

Finally, a sensitivity analysis was performed. This analysis shows that the process is highly sensitive to certain operating variables as P^f, T, C^{ftot}. In second place, the process is sensitive to design variables as L and Ro. Technological coefficients are also highly influential for the permeation process like the solute permeability constant: B. Therefore, a careful effort should be made to calculate accurately all the technological coefficients involved in the process.

Once the equations describing the process that takes place at each membrane module have been established in a future work this model will be incorporated into a design and synthesis desalination framework, including one or two stages. Equations relating the stages and establishing the general plant requirements, as well as cost equations will be formulated. An optimization problem will be defined in order to obtain the design and operating conditions for the reverse osmosis desalination network for different seawater salinities, with a given fresh water requirement and minimizing the cost per m^3 of product water.

Acknowledgements

The authors acknowledge financial supports from 'Consejo Nacional de Investigaciones Científicas y Técnicas' (CONICET) and 'Agencia Nacional de Promoción Científica y Tecnológica' (ANPCyT).

References

Al-Bastaki, N.M. and Abbas, A., 1999, Modeling an industrial reverse osmosis unit. Desalination, 126: 33–39.

Al-Bastaki, N.M. and Abbas, A., 2000, Predicting the performance of RO membranes. Desalination, 132: 181–187.

Avlonitis, S.A., Pappas, M. and Moutesidis, K., 2007, A unified model for the detailed investigation of membrane modules and RO plants performance. Desalination, 203: 218–228.

Brooke, A., Kendrick, D., Meeraus, A. and Raman, R., (1997). *GAMS Language Guide, Release 2.25, Version 92*. (GAMS Development Corporation).

Chatterjee, A., Ahluwalia, A., Senthilmurugan, S. and Gupta, S.K., 2004, Modeling of a radial flow hollow fiber module and estimation of model parameters using numerical techniques. J. Membr. Sci., 236: 1–16.

Costa, M.L. and Dickson, J.M., 1991, Modelling of modules and systems in reverse osmosis. Part I. Theoretical system design model development. Desalination, 80: 251–274.

Fletcher, D.F. and Wiley, D.E., 2004, A computational fluids dynamics study of buoyancy effects in reverse osmosis. J. Membr. Sci., 245: 175–181.

Hawlader, M.N.A., Ho, J.C. and Malek, A., 1994, An experimental and analytical study of permasep-B10 separation characteristics. J. Membr. Sci., 87: 1–21.

Jamal, K., Khan, M.A. and Kamil, M., 2004, Mathematical modeling of reverse osmosis systems. Desalination, 160: 29–42.

Kimura, S. and Sourirajan, S., 1967, Analysis of data in reverse osmosis with porous cellulose acetate membranes. AIChE J., 13: 497–503.

Kumano, A., Sekino, M., Matsui, Y., Fujiwara, N. and Matsuyama, H., 2008, Study of mass transfer characteristics for a hollow fiber reverse osmosis module. J. Membr. Sci., 324: 136–141.

Malek, A., Hawlader, M.N.A. and Ho, J.C., 1994, A lumped transport parameter approach in predicting B10 RO permeator performance. Desalination, 99: 19–38.

Marcovecchio, M.G., Aguirre, P.A. and Scenna, N.J., 2005, Global optimal design of reverse osmosis networks for seawater desalination: modeling and algorithm. Desalination, 184: 259–271.

Marriott, J. and Sørensen, E., 2003, The optimal design of membrane systems. Chem. Eng. Sci., 58: 4991–5004.

Marriott, J. and Sørensen, E., 2003, A general approach to modelling membrane modules. Chem. Eng. Sci., 58: 4975–4990.

Paul, D.R., 2004, Reformulation of the solution-diffusion theory of reverse osmosis. J. Membr. Sci., 241: 371–386.

Sekino, M., 1993, Precise analytical model of hollow fiber reverse osmosis modules. J. Membr. Sci., 85: 241–252.

Sekino, M., 1995, Study of an analytical model for hollow fiber reverse osmosis module systems. Desalination, 100: 85–97.

Smart, J., Starov, V.M. and Lloyd, D.R., 1996, Performance optimization of hollow fiber reverse osmosis membranes. Part II. Comparative study of flow configurations. J. Membr. Sci., 119: 117–128.

Starov, V.M., Smart, J. and Lloyd, D.R., 1995, Performance optimization of hollow fiber reverse osmosis membranes. Part I. Development of theory. J. Membr. Sci., 103: 257–270.

Villafafila, A. and Mujtaba, I.M., 2003, Fresh water by reverse osmosis based desalination: simulation and optimisation. Desalination, 155: 1–13.

Wiley, D.E. and Fletcher, D.F., 2003, Techniques for computational fluid dynamics modelling of flow in membrane channels. J. Membr. Sci., 211: 127–137.